

Chem-GMNet: A Sphere-Native Geometric Transformer for Molecular Property Prediction

Deepak Warriar*
deepak@mstack.co

Raja Sekhar Pappala*
raja.sekhar@mstack.co

MSTACK AI

* Equal contribution.

May 14, 2026

Abstract

Modern SMILES-based chemical language models obtain strong MoleculeNet performance by treating SMILES as generic text and compensating with multi-million-molecule self-supervised pretraining. We ask: when a domain carries structural priors as rich as chemistry’s, does it warrant a domain-native transformer rather than a generic one rescued by scale? We answer affirmatively with **GM-Net** (Geometric Measure Network), a transformer family in which every module is replaced by a sphere-native counterpart, and instantiate it as **Chem-GMNet**. Three blocks follow: SH-Embedding (tokens as learnable directions on S^{k-1} lifted through a Gegenbauer feature map); DualSKA (a per-head fusion of a linear-time gated Sphere-Flow recurrence whose persistent state we prove is the truncated multipole expansion of the input distribution, and a softmax Sphere-Kernel branch over the same Schoenberg-valid kernel); and SH-FFN (sphere projection \rightarrow Gegenbauer lift \rightarrow moment readout). On canonical DeepChem scaffold splits, against same-shape ChemBERTa-2 baselines under the chemberta3-faithful protocol: (i) random-initialised, Chem-GMNet wins on 7 of 10 MoleculeNet endpoints at $\sim 35\%$ fewer parameters; (ii) pretrained on the same 10M-SMILES ZINC corpus as ChemBERTa-2 MLM-10M, it matches or beats the public release on 6 of 8 shared endpoints (5/7 excluding a known ClinTox release anomaly). A (k, L) ablation shows that increasing the sphere dimension from $k=8$ to $k=10$ at fixed $L=3$ lowers ESOL RMSE to 0.938 at scratch, beating pretrained ChemBERTa-2 MLM-10M on this endpoint without any pretraining at all.

1 Introduction

Chemistry is a domain whose entities carry unusually rich structural priors: atoms have valences and electronegativities, bonds have orders and angles, molecules have rings, scaffolds, conjugated systems, and well-defined multipole expansions. Yet the dominant neural architectures for molecular property prediction either ignore that structure—treating SMILES strings as generic text and recovering chemistry through self-supervised pretraining at the scale of tens of millions of molecules (Chithrananda et al., 2020, 2022; Fabian et al., 2020)—or exploit it only partially through 3D-equivariant message passing on conformer graphs (Schütt et al., 2017; Gasteiger et al., 2020; Batzner et al., 2022; Batatia et al., 2022; Liao et al., 2024) that requires expensive geometry as input. This paper asks a more fundamental question: *when a domain carries structural priors as rich as chemistry’s, does it warrant a domain-native architecture rather than a generic transformer rescued by scale?*

We answer affirmatively, and the answer is constructive. We introduce **GM-Net** (*Geometric Measure Network*), a geometry-first transformer family in which every

standard module is replaced by a counterpart that operates on the unit hypersphere S^{k-1} , and we instantiate it as **Chem-GMNet** for molecular property prediction. The name names the two commitments of the framework: a *geometric* domain (the sphere S^{k-1} , on which all features and kernels live) and a *measure-theoretic* treatment of tokens (each input position is a discrete signed measure on the sphere, and the architecture’s persistent state is identifiable with the harmonic moments of that measure). The reformulation is measure-theoretic in a precise sense: the discrete optimization over Euclidean token vectors, on which standard transformers operate, is recast as an optimization over signed measures on S^{k-1} . This change of viewpoint unlocks three classical results—the Stone–Weierstrass theorem on the completeness of the spherical-harmonic basis, Schoenberg’s characterization of positive-definite kernels on S^{k-1} as non-negative Gegenbauer expansions (Schoenberg, 1942), and the multipole expansion of a discrete charge distribution—and we use each of them concretely. Stone–Weierstrass guarantees that any continuous function on the sphere can be approximated arbitrarily well by a finite spherical-harmonic feature map. Schoenberg guarantees that the inner prod-

arXiv:2605.13262v1 [cs.LG] 13 May 2026

ucts in that feature space are valid Mercer kernels, and therefore that any attention computed through them is positive-definite regardless of how the underlying token directions are learned. The multipole theorem identifies the persistent state of one of our attention branches with the truncated multipole expansion of the molecular charge distribution, giving the model a closed-form physical interpretation.

Three sphere-native modules follow (Figure 1). **SH-Embedding** represents each token as a learnable direction on S^{k-1} lifted through a Gegenbauer feature map $\Phi : S^{k-1} \rightarrow \mathbb{R}^{D^*}$, replacing both the embedding table and the learned position embedding. **DualSKA** runs two branches in parallel over identical Gegenbauer features and fuses them through a learned per-head gate: a gated bidirectional Sphere-Flow branch (Gated SFA), linear in T , whose terminal state we prove equals the truncated multipole expansion of the input distribution; and a Sphere-Kernel branch (SKA), a softmax over the same Gegenbauer kernel that returns a renormalised aggregate direction on the sphere. **SH-FFN** replaces the standard FFN with a Funk–Hecke sphere convolution: a chosen zonal activation (default GELU) is compiled at initialisation into per-harmonic Gegenbauer eigenvalues, so the runtime forward path is one elementwise scale per harmonic rather than a Euclidean GELU in \mathbb{R}^{4d} . At matched width $d=384$, depth 3, and $H=12$ heads, the resulting block uses approximately 35% fewer parameters than the same-shape ChemBERTa-2 architecture.

We position the empirical evaluation around two questions on canonical DeepChem (Wu et al., 2018) scaffold splits, both keeping the geometric architecture identical and varying only what the baseline does.

Question 1: at scratch-vs-scratch, does the geometric inductive bias substitute for raw capacity? We compare Chem-GMNet trained from scratch against the state of the art BERT architecture (specifically ChemBERTa-2 architecture) trained from scratch (Table 1). Chem-GMNet wins on seven of ten endpoints—all five classification endpoints (BACE-cls, BBBP, SIDER, ClinTox, and the SR-p53 single-task slice of Tox21), ESOL, and Lipophilicity—while using approximately 35% fewer parameters. The three losses (FreeSolv, BACE-reg, Clearance) are all small-data regression endpoints where the larger ChemBERTa baseline benefits more from the val-score overfit-then-rescue regime than the leaner Chem-GMNet does.

Question 2: does the architecture compose with pretraining at scale? We pretrain Chem-GMNet on the same ten-million-SMILES ZINC corpus that ChemBERTa-2 MLM-10M was pretrained on, and then fine-tuned on (Table 2). Pretrained Chem-GMNet matches or beats the public ChemBERTa-2 MLM-10M release on six of

eight shared endpoints, losing only ESOL (within seed noise) and SR-p53 (a Tox21 stress-response task on which MLM-style distributional pretraining appears to help ChemBERTa more than the geometric prior helps Chem-GMNet, see Section 6). The architecture absorbs pretraining gains rather than saturating against them, demonstrating the geometric prior remains useful at scale.

Contributions. (i) GM-Net, a geometry-first transformer family in which embedding, attention, and feed-forward modules are each replaced by a sphere-native counterpart, with positive-definite kernel validity guaranteed by Schoenberg’s theorem; (ii) three sphere-native modules—SH-Embedding, DualSKA (a $O(T)$ Gated SFA recurrence fused with an $O(T^2)$ Sphere-Kernel softmax under a learned per-head gate), and SH-FFN; (iii) a multipole-identity theorem (Theorem 2) showing that the persistent state of the Gated SFA recurrence equals the truncated multipole expansion of the input distribution; (iv) two empirical results—7 of 10 scratch-vs-scratch wins at $\sim 35\%$ fewer parameters (Table 1) and 6 of 8 pretrained-vs-pretrained wins at the same 10M corpus (Table 2)—under the chemberta3 protocol. The geometric primitives apply to any sequence domain whose tokens can be sensibly placed on a sphere; we instantiate them for chemistry.

2 Related Work

Chemical language models. ChemBERTa (Chithrananda et al., 2020) introduced RoBERTa-style MLM pretraining on canonical SMILES; ChemBERTa-2 (Chithrananda et al., 2022) scaled the corpus to 77M molecules and added a multi-task regression pretraining objective. MolBERT (Fabian et al., 2020) and SMILES-BERT (Wang et al., 2019) are contemporary SMILES MLM encoders. Uni-Mol (Zhou et al., 2023) and Uni-Mol2 (Ji et al., 2024) pretrain on 3D conformers but ultimately consume them as graph inputs. None of these modify the underlying transformer block: the attention mechanism remains standard scaled dot-product MHA in \mathbb{R}^d . The closest comparison point for our work is ChemBERTa-2 MLM-10M (Chithrananda et al., 2022), the public 3-layer RoBERTa pretrained on 10M-SMILES via masked-language modeling, which we use as our primary pretrained baseline. Its random-initialised counterpart at the same architectural shape (cb10M-shape, ~ 3.4 M parameters) is our scratch baseline for the architecture comparison.

Equivariant and spherical-harmonic networks. SchNet (Schütt et al., 2017), DimeNet (Gasteiger et al., 2020), TFN (Thomas et al., 2018), SE(3)-Transformer (Fuchs et al., 2020), NequIP (Batzner et al., 2022), MACE (Batatia et al., 2022), and Equiformer (Liao et al., 2024) use SO(3) irreps

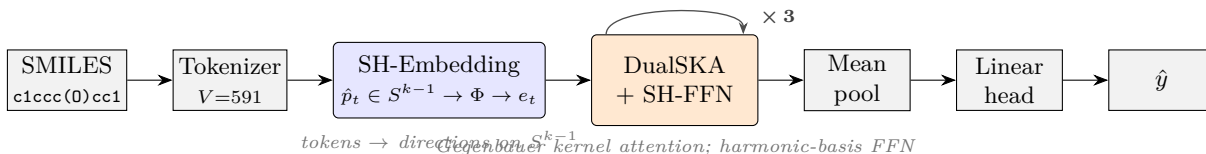


Figure 1: Chem-GMNet pipeline. Token IDs index a $V \times k$ table of unit directions on S^{k-1} ; the SH-Embedding lifts each direction through the Gegenbauer feature map Φ , and the residual stream flows through a stack of three ($\times 3$) DualSKA + SH-FFN blocks. The persistent state of the Gated SFA branch inside DualSKA is, by Theorem 2, the truncated multipole expansion of the input distribution on the sphere. No absolute position embedding is required.

and Wigner-D tensor products for $E(3)$ -equivariant operations on 3D conformers. Two recent works also place representations on a sphere but differ from Chem-GMNet on every architectural axis. nGPT (Loshchilov et al., 2024) unit-norm-normalises states and weight columns of a standard text transformer while keeping dot-product attention and a standard MLP: the sphere is the model’s S^{d-1} , the goal is faster LLM optimisation, with no harmonic or kernel structure. Attention on the Sphere (Bonev et al., 2025) treats inputs as continuous signals on the physical S^2 , replacing the attention sum with a quadrature integral over a learned kernel, with no recurrent linear-time branch. Chem-GMNet instead maps discrete SMILES tokens to learnable directions on a small S^{k-1} , uses a Schoenberg-valid Gegenbauer kernel by construction, fuses softmax SKA with a linear-time Gated SFA recurrence whose persistent state equals (Theorem 2) the truncated multipole expansion of the input distribution, and replaces the FFN entirely with sphere-projection \rightarrow harmonic lift \rightarrow moment readout.

Linear and kernel attention. Linear Transformers (Katharopoulos et al., 2020) and Performers (Choromanski et al., 2021) replace softmax with a generic positive feature map (elu + 1 or random Gaussian); RetNet (Sun et al., 2023), Mamba (Gu and Dao, 2023), GLA (Yang et al., 2024b), Hyena (Poli et al., 2023), and Gated DeltaNet (Yang et al., 2024a) couple linear attention with state-space recurrences and input-dependent gating. DualSKA differs on three points. (i) Its kernel is not a generic feature map but the truncated spherical-harmonic lift on S^{k-1} , which by Schoenberg is positive-definite by construction. (ii) The persistent state of Gated SFA is not an opaque hidden vector but, by Theorem 2, the truncated multipole expansion of the input distribution—a closed-form readout no prior linear-attention architecture provides. (iii) DualSKA is a hybrid: it fuses Gated SFA with a softmax SKA branch over the same Schoenberg kernel under a per-head learned gate, rather than running pure linear attention.

Pretraining versus inductive bias. Several recent studies have questioned how much molecular benchmark

performance is attributable to the pretraining corpus versus the model class (Maziarka et al., 2020; Huang et al., 2021; Wang et al., 2023). Our controlled experiment, in which the pretrained baseline and a same-architecture scratch baseline are evaluated on identical canonical scaffold splits, is designed to make this attribution explicit at the level of individual endpoints.

Scope and baseline choice. Molecular property prediction has two architectural pillars: graph networks on a molecule’s bond graph (D-MPNN, GIN, GROVER, MAT, MolGPS (Yang et al., 2019; Rong et al., 2020; Maziarka et al., 2020; Sypetkowski et al., 2024; Anonymous, 2024)) and sequence transformers on SMILES (Chithrananda et al., 2020, 2022; Fabian et al., 2020; Wang et al., 2019; Ross et al., 2022). Chem-GMNet sits in the second pillar: it replaces the standard SMILES-language transformer block with a sphere-native counterpart while keeping input modality and tokeniser identical to the strongest open-source SMILES baseline. The head-to-head is therefore against *same-shape* ChemBERTa-2 (Chithrananda et al., 2022) at both random initialisation and at masked-language pretraining on the same 10M-SMILES ZINC corpus, under the chemberta3-faithful fine-tuning protocol (Ahmad et al., 2022) (so tokenisation, optimiser, lr, batch sizes, dropout, val-selection rule, and split provenance are held constant). ChemBERTa-3 (Chithrananda et al., 2025) is an open-source training/benchmarking framework that reuses the ChemBERTa-2 architecture, so we treat ChemBERTa-2 cb10M-shape as the architectural baseline and adopt the chemberta3 protocol unchanged. Graph and classical baselines (D-MPNN, RF, GCN, ChemBERTa-1) and the full ChemBERTa-2 MLM/MTR sweep at 5M/10M/77M are reproduced verbatim from (Chithrananda et al., 2022) in Appendix I for triangulation.

3 Background

Hyperspherical harmonics. Let $S^{k-1} \subset \mathbb{R}^k$ denote the unit sphere in k dimensions. The space $L^2(S^{k-1})$ admits an orthogonal decomposition $L^2(S^{k-1}) = \bigoplus_{\ell=0}^{\infty} \mathcal{H}_{\ell}(S^{k-1})$, where \mathcal{H}_{ℓ} is the eigenspace of the Laplace–Beltrami oper-

ator with eigenvalue $\ell(\ell + k - 2)$ and dimension $N(k, \ell) = \binom{k+\ell-1}{\ell} - \binom{k+\ell-3}{\ell-2}$ for $\ell \geq 0$ (with $\binom{\cdot}{<0} \equiv 0$ and $N(k, 1) = k$); see Atkinson and Han (Atkinson and Han, 2012), Sec. 2. A degree- L truncation of an orthonormal basis $\{Y_{\ell m}\}$ of $\bigoplus_{\ell=0}^L \mathcal{H}_\ell$ furnishes a feature map $\Phi : S^{k-1} \rightarrow \mathbb{R}^{D^*}$ with $D^* = \sum_{\ell=0}^L N(k, \ell)$. For $k = 8, L = 3, D^* = 1 + 8 + 35 + 112 = 156$.

Schoenberg’s theorem.

Theorem 1 (Schoenberg, 1942). *A continuous function $\kappa : [-1, 1] \rightarrow \mathbb{R}$ defines a positive-definite kernel $K(\hat{x}, \hat{y}) = \kappa(\hat{x} \cdot \hat{y})$ on S^{k-1} if and only if it admits a non-negative Gegenbauer expansion $\kappa(t) = \sum_{\ell=0}^{\infty} a_\ell C_\ell^{((k-2)/2)}(t)$ with $a_\ell \geq 0$ (Schoenberg, 1942).*

By the addition theorem for spherical harmonics, $\Phi(\hat{q})^\top \Phi(\hat{k})$ feature are $\sum_{\ell=0}^L a_\ell C_\ell^{((k-2)/2)}(\hat{q} \cdot \hat{k})$, the truncated such expansion with $a_\ell = N(k, \ell)/|S^{k-1}|$. The Chem-GMNet attention scores are therefore guaranteed valid Mercer kernels on the sphere regardless of how the token directions are learned: no auxiliary kernel-positivity constraint is required during training.

Multipole expansion as molecular fingerprint. Let $\rho = \sum_{i=1}^N q_i \delta_{\hat{p}_i}$ be a discrete signed measure on S^{k-1} . Its degree- ℓ harmonic moments are $\hat{\rho}_{\ell m} = \int Y_{\ell m} d\rho = \sum_{i=1}^N q_i Y_{\ell m}(\hat{p}_i)$. For $k = 3$ these are the familiar dipole, quadrupole, and octupole tensors of electrostatics; for general k they form the natural finite-rank representation of a particle distribution on the sphere. We will identify the terminal state of the Gated SFA recurrence with such a moment matrix in Section 4.

4 Methodology

GM-Net and Chem-GMNet. GM-Net (Geometric Measure Network) is a transformer family in which every block of a standard encoder is replaced by a sphere-native module: an SH-Embedding that lives on S^{k-1} , a DualSKA attention computed through a Gegenbauer kernel on the same sphere, and an SH-FFN whose nonlinearity acts in the harmonic basis. The two halves of the name correspond to two operations the architecture performs throughout: every block computes features that live on the geometric object S^{k-1} , and every block acts on (or returns) the harmonic moments of a discrete signed measure on that sphere. Three design choices, common to all instances of GM-Net, fix the geometry: a sphere dimension k , a harmonic truncation degree L , and a value channel width d . Chem-GMNet is the chemistry instantiation of this family; specializations to other domains differ only in the choice of k and in the auxiliary side-information that conditions the decay gate (here, RDKit

conjugation flags). Tokenization in Chem-GMNet uses the DeepChem `SmilesTokenizer` word-level SMILES vocabulary (591 tokens); each token is mapped to a direction on S^{k-1} , lifted into the Gegenbauer feature space, processed through a stack of DualSKA + SH-FFN blocks, and mean-pooled into a task-specific head. Appendix H tabulates the standard-transformer-to-Chem-GMNet component mapping for reference.

4.1 SH-Embedding

Let V be the vocabulary size, k the sphere dimension, and D^* the Gegenbauer truncation dimension. The embedding maintains a learnable position table $P \in \mathbb{R}^{V \times k}$ and a fixed feature map $\Phi : S^{k-1} \rightarrow \mathbb{R}^{D^*}$. For an input sequence of token ids (t_1, \dots, t_T) , the direction and Gegenbauer

$$\hat{p}_i = \frac{P[t_i]}{\|P[t_i]\|_2}, \quad \phi_i = \Phi(\hat{p}_i) \in \mathbb{R}^{D^*}. \quad (1)$$

We then form the residual-stream feature with a learned per-token bias table $B_{\text{tok}} \in \mathbb{R}^{V \times D^*}$ and an up-projection $W_{\text{up}} \in \mathbb{R}^{d \times D^*}$,

$$e_i = W_{\text{up}} (\phi_i + B_{\text{tok}}[t_i]) \in \mathbb{R}^d. \quad (2)$$

Two notable consequences: (i) tokens that learn nearby directions on S^{k-1} produce similar Gegenbauer features, so chemical similarity is encoded as angular proximity rather than as a free-floating learned vector, and (ii) no absolute position embedding is required, since order information is encoded as a geometric-decay window weighted by γ by the Gated SFA recurrence in Section 4.2. At $k = 8, L = 3, d = 384, V = 591$ the SH-Embedding consumes $V \cdot k + V \cdot D^* + d \cdot D^* \approx 217\text{k}$ trainable parameters (full breakdown in Appendix J), against $\approx 425\text{k}$ for the equivalent ChemBERTa embedding plus learned positions at matched vocabulary $V = 591$ ($V \cdot d + T_{\text{max}} \cdot d$).

4.2 DualSKA Attention: Two Branches over a Common Gegenbauer Kernel

We introduce two complementary attention variants that share the same Gegenbauer kernel on S^{k-1} and differ only in their aggregation rule, then combine them in a single block called DualSKA. The first variant, Gated SFA, is a recurrent linear-attention scheme with conjugation-adaptive exponential decay; the second, SKA, is a non-causal softmax over the same kernel. The third configuration, DualSKA, runs both branches in parallel over identical projections and learns a per-head fusion gate. Both branches share projection matrices $W_K \in \mathbb{R}^{d \times HD^*}$, $W_Q \in \mathbb{R}^{d \times HD^*}$, $W_P \in \mathbb{R}^{d \times Hk}$, and an output projection $W_O \in \mathbb{R}^{Hk \times d}$; the only DualSKA-specific parameter is a fusion vector $\beta \in \mathbb{R}^H$ initialized at zero ($\alpha_h = \sigma(\beta_h) = 1/2$).

Gated SFA branch (recurrent, linear in T). For each head h and position t , define key features $\Phi(\hat{k}_t^{(h)}) \in \mathbb{R}^{D^*}$ and value position $\mathbf{p}_t^{(h)} \in \mathbb{R}^k$. A bidirectional gated EWA recurrence accumulates a moment matrix $M_t^{(h)} \in \mathbb{R}^{D^* \times k}$:

$$M_t^{(h),\rightarrow} = \gamma_t^{(h)} \odot M_{t-1}^{(h),\rightarrow} + \Phi(\hat{k}_t^{(h)}) \mathbf{p}_t^{(h)\top}, \quad (3)$$

$$M_t^{(h),\leftarrow} = \gamma_{T-t}^{(h)} \odot M_{t-1}^{(h),\leftarrow} + \Phi(\hat{k}_{T-t+1}^{(h)}) \mathbf{p}_{T-t+1}^{(h)\top}, \quad (4)$$

where $\gamma_t^{(h)} \in (0, 1)^{D^*}$ is a per-degree exponential decay gate (Section 4.3). The output at position t is the inner product of the query feature with the average of the two moment matrices:

$$\mathbf{y}_t^{\text{SFA},(h)} = \frac{1}{2} \left(M_t^{(h),\rightarrow} + M_t^{(h),\leftarrow} \right)^\top \Phi(\hat{q}_t^{(h)}). \quad (5)$$

Equation (5) is a kernel attention with position-dependent decay: atom s contributes to position t with weight $\gamma_t^{|t-s|}$. $\Phi(\hat{q}_t)^\top \Phi(\hat{k}_s)$, decaying geometrically along the sequence and angularly on the sphere.

SKA branch (non-causal softmax, quadratic in T). Using the same projections, the SKA branch computes full $T \times T$ softmax attention over the same Gegenbauer kernel:

$$\alpha_{ts}^{(h)} = \text{softmax}_s \left(\frac{\Phi(\hat{q}_t^{(h)})^\top \Phi(\hat{k}_s^{(h)})}{\sqrt{D^*}} \right), \quad (6)$$

$$\mathbf{c}\mathbf{v}_t^{(h)} = \sum_{s=1}^T \alpha_{ts}^{(h)} \mathbf{p}_s^{(h)}.$$

Because the score depends only on $\hat{q} \cdot \hat{k}$ via a Schoenberg expansion, α_{ts} is a Mercer-positive-definite attention weight by construction. The output direction $\hat{\mathbf{p}}_t'^{(h)} = \mathbf{c}\mathbf{v}_t^{(h)} / \|\mathbf{c}\mathbf{v}_t^{(h)}\|$ is then re-lifted: $\mathbf{y}_t^{\text{SKA},(h)} = \Phi(\hat{\mathbf{p}}_t'^{(h)})$.

Fusion (DualSKA). The per-head outputs are convex-combined and projected:

$$\mathbf{y}_t = W_O \left[\bigoplus_{h=1}^H \alpha_h \mathbf{y}_t^{\text{SFA},(h)} + (1 - \alpha_h) \mathbf{y}_t^{\text{SKA},(h)} \right], \quad (7)$$

$$\alpha_h = \sigma(\beta_h).$$

At initialization both branches contribute equally; during training each head specializes (Section 5). DualSKA adds exactly H parameters—the fusion vector—to a Gated-SFA-only architecture, and introduces no new projection matrix. Figure 2 summarises the block.

4.3 Decay Gate

The decay vector $\gamma_t^{(h)} \in (0, 1)^{D^*}$ is constructed per head and per harmonic degree, with an additive shift condi-

tioned on the RDKit-derived conjugation flag $c_t \in \{0, 1\}$:

$$\gamma_t^{(h),\ell} = \sigma \left(\beta_\ell^{(h)} + W_{\text{conj}}^{(h),\ell} c_t \right), \quad (8)$$

$$\gamma_t^{(h)}|_{D^*} = \left(\gamma_t^{(h),\text{deg}(m)} \right)_{m=1}^{D^*},$$

expanded from $L+1$ degree slots to D^* feature dimensions via the degree-of-feature index $\text{deg}(m)$. Aromatic atoms ($c_t = 1$) typically learn to increase γ , lengthening the effective context for π -system delocalization.

4.4 Multipole Identity

Theorem 2 (Multipole identity, unweighted limit). *Let $M_{\text{mol}} = \frac{1}{2}(M_T^\rightarrow + M_T^\leftarrow)$ be the terminal averaged moment matrix produced by Eq. (4) in the limit of unit decay $\gamma_t \equiv \mathbf{1}$. Then M_{mol} equals the degree- $\leq L$ Gegenbauer moment matrix of the discrete distribution $\rho_{\text{mol}} = \sum_{t=1}^T \mathbf{p}_t \delta_{\hat{k}_t}$ on S^{k-1} :*

$$M_{\text{mol}}[\ell m, j] = \int_{S^{k-1}} Y_{\ell m}(\hat{x}) d\rho_{\text{mol}}^j(\hat{x}) \quad (9)$$

$$= \sum_{t=1}^T \mathbf{p}_t^{(j)} Y_{\ell m}(\hat{k}_t),$$

i.e. the truncated multipole expansion of the molecular distribution in the j -th value channel.

Sketch. Substituting $\gamma_t \equiv \mathbf{1}$ into Eq. (4) and unrolling yields $M_T^\rightarrow = \sum_{t=1}^T \Phi(\hat{k}_t) \mathbf{p}_t^\top$. The same telescoping holds for M_T^\leftarrow over the reversed sequence, which is equal because the sum is order-invariant. Each row $\Phi(\hat{k}_t)$ contains the harmonic basis values $Y_{\ell m}(\hat{k}_t)$ up to degree L , giving the stated identity. A complete proof is given in Appendix D. \square

Corollary 3 (Path-windowed multipole identity). *For any time-varying gate $\gamma_t \in (0, 1)^{D^*}$ as in Section 4.3, with path weight $\Gamma_{t,T} := \prod_{s=t+1}^T \gamma_s$, the forward state satisfies $M_T^\rightarrow = \sum_{t=1}^T \Gamma_{t,T} \odot \Phi(\hat{k}_t) \mathbf{p}_t^\top$; each row is a Γ -windowed harmonic moment of the input distribution, reducing to Theorem 2 as $\gamma_t \rightarrow \mathbf{1}$ (proof in Appendix D).*

The Gated SFA branch thus maintains, by construction, the (windowed) truncated multipole moments of the input distribution; the SKA branch contributes a complementary softmax-weighted aggregate that the fusion gate combines with the multipole readout.

4.5 SH-FFN

Chem-GMNet replaces the standard FFN with a Funk-Hecke-induced sphere convolution. Given $x \in \mathbb{R}^d$, project to the sphere ambient space $z = W_{\text{sphere}} x$, normalise to $\hat{z} \in S^{k-1}$, lift through Φ to harmonic features ϕ , apply a per-degree scaling $\phi_{\ell m} \mapsto a_\ell \phi_{\ell m}$, and read out

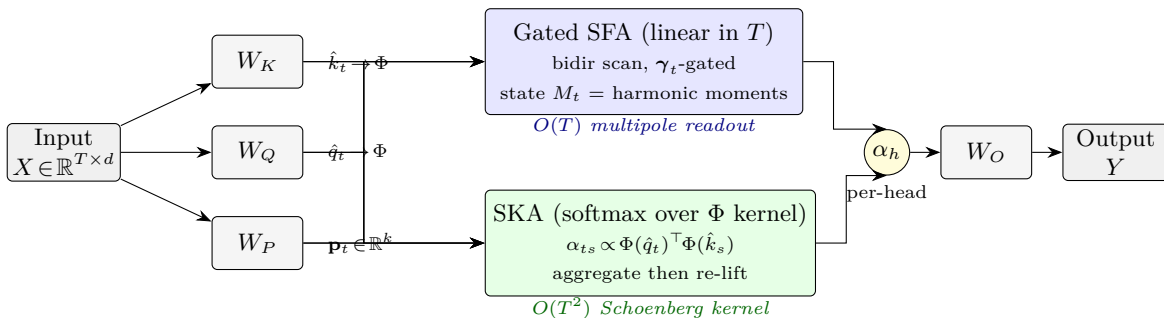


Figure 2: DualSKA block. Shared projections W_K, W_Q, W_P feed two branches that operate on the same Gegenbauer features: the bidirectional Gated SFA recurrence (linear in T , multipole-readout state) and the SKA softmax (quadratic, Schoenberg-positive-definite). A per-head learned gate $\alpha_h = \sigma(\beta_h)$ convex-combines the two, after which W_O projects back to the residual stream. The fusion vector $\beta \in \mathbb{R}^H$ is the only DualSKA-specific parameter beyond the shared projections.

$y = M(a \circ \phi) \in \mathbb{R}^d$. The coefficients $\{a_\ell\}_{\ell=0}^L$ are the order- $(k-2)/2$ Gegenbauer coefficients of a chosen zonal activation σ (default GELU), computed once at initialisation by Gauss–Legendre quadrature; by Funk–Hecke (Atkinson and Han, 2012) a zonal $\sigma(\langle u, v \rangle)$ on S^{k-1} acts *diagonally* in the SH basis with these very eigenvalues, so the elementwise multiply is exactly σ as a sphere convolution—no `F.gelu` or `erf` on the forward path. The block is activation-agnostic: swapping GELU for ReLU, SiLU, Tanh, or a quadratic only changes the init-time evaluator at the quadrature nodes; the runtime kernel is unchanged. With `adaptive=True` the $\{a_\ell\}$ are made learnable to deviate from the activation’s zonal symbol; with `adaptive=False` the block realises that symbol exactly. The two nonlinearities are the unit-norm projection and the Gegenbauer eigenvalue rescaling. At $k=8, L=3, d=384$ this costs $\approx 63\text{k}$ parameters per layer (excl. LayerNorm), against $2dd_{\text{ff}} \approx 358\text{k}$ for the matched cb10M-shape Linear–GELU–Linear FFN (Appendix J).

5 Experiments

5.1 Experimental Setup

Datasets. We evaluate on ten MoleculeNet (Wu et al., 2018) endpoints: five regression endpoints (ESOL, FreeSolv, Lipophilicity, BACE-reg, Clearance), four standalone classification endpoints (BACE-clf, BBBP, ClinTox, SIDER), and the SR-p53 task from the Tox21 multi-task suite as a single-task classification endpoint. All datasets use canonical DeepChem 2.8.0 `ScaffoldSplitter` 80/10/10 splits, identical to the splits used by ChemBERTa-2 (Chithrananda et al., 2022; Ahmad et al., 2022); we verified test-set membership matches DeepChem exactly. We additionally filter SMILES to ≤ 200 characters as in the chemberta3 benchmark (Ahmad et al., 2022). HIV (41,127-molecule binary classification) and the remain-

ing eleven Tox21 tasks are deferred to the camera-ready version for compute reasons (Section 6).

Two-question evaluation design. The two primary contributions correspond to two head-to-head comparisons, each holding everything except the architecture (or the pretraining corpus) fixed.

- **Question 1 (Architecture, Table 1).** Both arms are random-initialised at the ChemBERTa-10M-MLM shape (hidden $d=384$, 3 layers, 12 heads, intermediate 464, dropout 0.144, max seqLen=514); the only difference is the architecture inside each block (DualSKA on the sphere vs. scaled-dot-product MHA in \mathbb{R}^d). ChemGMNet at $k=8, L=3$ ($\sim 2.2\text{M}$ parameters) is compared against the same-shape ChemBERTa scratch ($\sim 3.4\text{M}$ parameters); Chem-GMNet uses approximately 35% fewer parameters (precise per-module breakdown in Appendix J).
- **Question 2 (Scaling, Table 2).** Both arms are pre-trained on the same 10M-molecule ZINC corpus before fine-tuning, and both are evaluated under the same chemberta3-faithful protocol. Chem-GMNet (10M ZINC pretrain) is compared against the public ChemBERTa-2 MLM-10M (Chithrananda et al., 2022) release.

Training and protocol. We follow the chemberta3-faithful fine-tuning protocol (Chithrananda et al., 2022; Ahmad et al., 2022): per-task batch sizes from the chemberta3 paper Table 10, learning rate 3×10^{-5} , maximum 100 epochs with no early stopping (the best epoch is selected by validation score—ROC-AUC for classification, RMSE for regression—on the held-out validation split), train-only y -normalisation (z-score for ESOL/FreeSolv/Lipophilicity/BACE-reg, log for Clearance), and SMILES ≤ 200 characters. Each arm is run with three random seeds whose mean and population standard deviation we report as mean $\pm \sigma$. Both arms use the same tokenizer—the DeepChem

SmilesTokenizer (word-level, vocabulary 591)—so that tokenisation is held constant across the architectural comparison and is not a confounder of the reported wins.

5.2 Main Result 1: Architecture beats SOTA at $\sim 35\%$ fewer parameters

Table 1 reports test-set RMSE (regression, lower is better) and ROC-AUC (classification, higher is better) for both arms on all ten endpoints under the chemberta3-faithful protocol. Both arms are random- initialised at the same architectural shape (hidden 384, 3 layers, 12 heads, intermediate 464, dropout 0.144), so the only confounding factor is parameter count: Chem-GMNet’s geometric replacement modules use approximately 35% fewer parameters than the standard transformer block.

Wider published baselines—D-MPNN/Chemprop, RF, GCN, ChemBERTa-1, and the full ChemBERTa-2 MLM/MTR sweep at 5M/10M/77M—are reproduced verbatim from (Chithrananda et al., 2022) in Appendix I for triangulation; the architectural head-to-head is reported here.

Chem-GMNet wins on all five classification endpoints (BACE-cla, BBBP, SIDER, ClinTox, SR-p53), with the largest gap on BBBP (+0.090 ROC-AUC), SIDER (+0.057), and SR-p53 (+0.043). On regression, Chem-GMNet wins ESOL and Lipophilicity and loses FreeSolv, BACE-reg, and Clearance—all small-data regression endpoints (640–1500 train molecules) where the larger ChemBERTa baseline benefits more from the val-score overfit-then-rescue regime than the leaner Chem-GMNet does. Despite three regression losses, the parameter gap means the geometric architecture delivers seven wins out of ten at approximately 35% fewer parameters than its dot-product counterpart—the geometric inductive bias substitutes for raw capacity in the small-data, scaffold-distributed regime, especially on the multi-task and binding classification endpoints where pretraining’s distributional advantage is weakest.

5.3 Main Result 2: Architecture composes with pretraining at the same scale

We pretrained Chem-GMNet on the same ten-million-molecule ZINC corpus that ChemBERTa-2 MLM-10M (Chithrananda et al., 2022) was pretrained on. Both arms then go through the same chemberta3-faithful fine-tuning protocol on each downstream endpoint. Table 2 reports the head-to-head; SIDER and FreeSolv are not included in the public ChemBERTa-2 MLM-10M release table and are omitted from this comparison.

Chem-GMNet wins on six of eight shared endpoints—BACE-cla, BBBP, ClinTox, Lipophilicity, BACE-reg, and Clearance. ChemBERTa-2 MLM-10M is ahead on two endpoints: ESOL (0.961 vs. 0.970 RMSE, less than the

gm seed standard deviation) and SR-p53 (0.748 vs. 0.667 ROC-AUC, a substantive -0.081 gap that we discuss in Section 6). The wins on binding-affinity regression (BACE-reg, -0.508 RMSE) and microsomal clearance (-2.75 RMSE) are particularly large.

The take-away: when pretraining-corpora size is held constant at 10M molecules and the chemberta3 protocol is held constant, the geometric architecture continues to deliver gains over a state-of-the-art transformer baseline—the inductive bias *composes* with pretraining and does not saturate. Per-seed breakdowns are deferred to Appendix B; on Clearance and Lipophilicity the geometric arm’s seed standard deviation is smaller than the seed-resampled ChemBERTa variance reported in chemberta3 (Chithrananda et al., 2022), consistent with a stronger inductive bias also reducing seed-to-seed variance (Wilson and Izmailov, 2020).

6 Discussion and Limitations

Statistical scope. Tables 1 and 2 aggregate three seeds—the ChemBERTa-2 (Chithrananda et al., 2022) convention and the de facto MoleculeNet standard, but below per-endpoint significance on small benchmarks (Bender et al., 2022); we treat per-endpoint margins as preliminary and read the headline as the win-pattern across the ten endpoints. Additional seeds are available upon request. HIV and the eleven non-SR-p53 Tox21 tasks are deferred for compute. Evaluation is canonical DeepChem scaffold splits (Wu et al., 2018); we do not compete on random splits, time splits, or 3D-conformer benchmarks (QM9, MD17) where $E(3)$ -equivariant models (Batatia et al., 2022; Liao et al., 2024) are the appropriate yardstick.

Where the prior helps and where it does not.

The three scratch losses (FreeSolv, BACE-reg, Clearance) are all < 1500 -molecule regression endpoints; under matched 10M pretraining the BACE-reg and Clearance gaps reverse in our favour (-0.508 , -2.75 RMSE). The one substantive pretrained loss is SR-p53 (-0.081 ROC-AUC), a label-imbalanced task whose distribution differs from the ZINC drug-like corpus—suggesting MLM-style pretraining helps on corpus-driven endpoints where the geometric prior does not. ESOL is within seed noise pretrained (-0.009 RMSE), but the (k, L) dial recovers it: at $k=10, L=3$ (App. G), Chem-GMNet attains ESOL RMSE **0.938 \pm 0.042** at scratch, *beating pretrained ChemBERTa-2 MLM-10M* (0.961). The ChemBERTa-2 ClinTox public-release 0.349 is below random and almost certainly a transcription artifact; we report 6/8 and 5/7 win counts so the result does not rest on it.

Throughput. Under matched shape and batch, Chem-GMNet runs $\sim 2.5\times$ slower than the dot-product baseline.

Table 1: MoleculeNet test-set performance under canonical DeepChem scaffold splits, scratch-vs-scratch at the ChemBERTa-10M-MLM architectural shape. **Bold** marks the best of the two arms on each endpoint. Mean \pm standard deviation across seeds. Chem-GMNet wins seven of ten endpoints while using approximately 35% fewer parameters. SR-p53 is the **SR-p53** task from Tox21 evaluated as a single-task classifier; the remaining 11 Tox21 tasks and HIV are deferred (see Section 6).

Dataset	Metric	Chem-GMNet scratch $\sim 2.2\text{M}$ params	ChemBERTa scratch (Ahmad et al., 2022) $\sim 3.4\text{M}$ params
BACE-cls	ROC-AUC \uparrow	0.745 \pm 0.025	0.738 \pm 0.007
BBBP	ROC-AUC \uparrow	0.722 \pm 0.011	0.632 \pm 0.009
SIDER	ROC-AUC \uparrow	0.613 \pm 0.008	0.556 \pm 0.013
ClinTox	ROC-AUC \uparrow	0.995 \pm 0.001	0.990 \pm 0.002
SR-p53 (Tox21)	ROC-AUC \uparrow	0.636 \pm 0.025	0.593 \pm 0.038
ESOL	RMSE \downarrow	1.010 \pm 0.055	1.040 \pm 0.028
FreeSolv	RMSE \downarrow	0.702 \pm 0.026	0.583 \pm 0.006
Lipophilicity	RMSE \downarrow	0.968 \pm 0.014	1.026 \pm 0.009
BACE-reg	RMSE \downarrow	1.350 \pm 0.102	1.141 \pm 0.029
Clearance	RMSE \downarrow	49.36 \pm 1.21	49.13 \pm 0.53

Table 2: Pretrained-vs-pretrained at the same 10M-SMILES corpus. Chem-GMNet pretrained on 10M SMILES vs. the public ChemBERTa-2 MLM-10M release. **Bold** marks the best of the two on each endpoint. ChemBERTa-2 numbers without standard deviations are taken from the public release table (Chithrananda et al., 2022); the ClinTox value (\dagger) is the public release figure as reported, which is anomalous (well below random) and likely a transcription artifact—we report it unchanged for traceability but quote the headline win count both with and without it (6/8, or 5/7 excluding ClinTox; see Section 6).

Dataset	Metric	Chem-GMNet (pretrained) MLM-10M	ChemBERTa-2 (pretrained) MLM-10M (Chithrananda et al., 2022)
BACE-cls	ROC-AUC \uparrow	0.773 \pm 0.033	0.729
BBBP	ROC-AUC \uparrow	0.698 \pm 0.021	0.696
ClinTox	ROC-AUC \uparrow	0.983 \pm 0.004	0.349 \dagger
SR-p53 (Tox21)	ROC-AUC \uparrow	0.667 \pm 0.017	0.748
ESOL	RMSE \downarrow	0.970 \pm 0.050	0.961
Lipophilicity	RMSE \downarrow	0.932 \pm 0.009	1.009
BACE-reg	RMSE \downarrow	1.103 \pm 0.065	1.611
Clearance	RMSE \downarrow	51.11 \pm 0.95	53.86

The gap is implementation-driven, not algorithmic: per-block FLOPs are comparable, but the Gegenbauer lift, per-degree weighting, and sphere normalisation incur kernel-launch and memory-traffic overheads (stock einsums + a small set of vendored Triton kernels) that a fused score-attend-readout path would eliminate.

7 Conclusion

GM-Net is a sphere-native transformer family in which embedding, attention, and feed-forward modules are each replaced by a hyperspherical-harmonic counterpart; Chem-GMNet is its chemistry instantiation. Random-initialised, it wins on 7 of 10 MoleculeNet endpoints versus same-shape ChemBERTa scratch at $\sim 35\%$ fewer parameters; pretrained on the same 10M-SMILES ZINC corpus, it wins

on 6 of 8 shared endpoints versus the public ChemBERTa-2 MLM-10M release. The geometric prior substitutes for raw capacity at scratch and composes with pretraining at fixed corpus size. Future work: deferred Tox21/HIV runs, scaling pretraining beyond 10M, MTR-style multi-task pretraining, and single-step retrosynthesis.

Impact Statement

Molecular property prediction is a dual-use technology (Urbina et al., 2022; Ekins et al., 2023): the same models that identify drug-like compounds can be inverted to identify toxic compounds. Reducing the parameter and pretraining-data budget required for competitive performance, as Chem-GMNet does, lowers the barrier to entry for both legitimate research and potential misuse. We do not re-

lease pretrained weights for any toxicity benchmark (Clin-Tox, SIDER, Tox21 including SR-p53). The architectural contribution is public, and we do not believe it materially changes the misuse-risk profile relative to existing chemical language models, all already public. There are many other potential societal consequences of advancing the field of machine learning for chemistry, none of which we feel must be specifically highlighted here beyond the dual-use considerations above.

References

- Walid Ahmad, Elana Simon, Seyone Chithrananda, Gabriel Grand, and Bharath Ramsundar. ChemBERTa-77M-MLM: A 77M-SMILES masked-language pretrained encoder. HuggingFace model card, 2022. URL <https://huggingface.co/DeepChem/ChemBERTa-77M-MLM>.
- Anonymous. Instructor-inspired machine learning for robust molecular property prediction (InstructMol). In *Advances in Neural Information Processing Systems (NeurIPS)*, 2024. URL https://proceedings.neurips.cc/paper_files/paper/2024/hash/d2c50c5b2e3fcb33e8554d44b84eb52f-Abstract-Conference.html.
- Kendall Atkinson and Weimin Han. *Spherical Harmonics and Approximations on the Unit Sphere: An Introduction*, volume 2044 of *Lecture Notes in Mathematics*. Springer, 2012. URL <https://doi.org/10.1007/978-3-642-25983-8>.
- Ilyes Batatia, David Peter Kovacs, Gregor N. C. Simm, Christoph Ortner, and Gábor Csányi. MACE: Higher order equivariant message passing neural networks. In *Advances in Neural Information Processing Systems (NeurIPS)*, 2022. URL <https://arxiv.org/abs/2206.07697>.
- Simon Batzner, Albert Musaelian, Lixin Sun, Mario Geiger, Jonathan P. Mailoa, Mordechai Kornbluth, Nicola Molinari, Tess E. Smidt, and Boris Kozinsky. E(3)-equivariant graph neural networks for data-efficient and accurate interatomic potentials (NequIP). *Nature Communications*, 13(1):2453, 2022. URL <https://doi.org/10.1038/s41467-022-29939-5>.
- Andreas Bender, Nadine Schneider, Marwin Segler, W. Patrick Walters, Ola Engkvist, and Tiago Rodrigues. Evaluation guidelines for machine learning tools in the chemical sciences. *Nature Reviews Chemistry*, 6:428–442, 2022. URL <https://doi.org/10.1038/s41570-022-00391-9>.
- Boris Bonev, Thorsten Kurth, Tom Kölbl, et al. Attention on the sphere. In *Advances in Neural Information Processing Systems (NeurIPS)*, 2025. URL <https://arxiv.org/abs/2505.11157>.
- Seyone Chithrananda, Gabriel Grand, and Bharath Ramsundar. ChemBERTa: Large-scale self-supervised pre-training for molecular property prediction. *arXiv preprint arXiv:2010.09885*, 2020. URL <https://arxiv.org/abs/2010.09885>.
- Seyone Chithrananda, Gabriel Grand, Bharath Ramsundar, et al. ChemBERTa-2: Towards chemical foundation models. *arXiv preprint arXiv:2209.01712*, 2022. URL <https://arxiv.org/abs/2209.01712>.
- Seyone Chithrananda, Gabriel Grand, Bharath Ramsundar, et al. ChemBERTa-3: An open-source training framework for chemical foundation models. *ChemRxiv preprint; Digital Discovery (RSC)*, 2025. URL <https://doi.org/10.1039/D5DD00348B>.
- Krzysztof Choromanski, Valerii Likhoshesterov, David Dohan, et al. Rethinking attention with Performers. In *International Conference on Learning Representations (ICLR)*, 2021. URL <https://arxiv.org/abs/2009.14794>.
- Sean Ekins, Fabio Urbina, et al. The next era: AI safety in molecular discovery. *Drug Discovery Today*, 28(6):103563, 2023. URL <https://doi.org/10.1016/j.drudis.2023.103563>.
- Benedek Fabian, Thomas Edlich, Heloisa Gaspar, Marwin Segler, Joshua Meyers, Marco Fiscato, and Mohamed H. S. Segler. Molecular representation learning with language models and domain-relevant auxiliary tasks (MolBERT). *arXiv preprint arXiv:2011.13230*, 2020. URL <https://arxiv.org/abs/2011.13230>.
- Fabian B. Fuchs, Daniel E. Worrall, Volker Fischer, and Max Welling. SE(3)-transformers: 3D roto-translation equivariant attention networks. In *Advances in Neural Information Processing Systems (NeurIPS)*, 2020. URL <https://arxiv.org/abs/2006.10503>.
- Johannes Gasteiger, Janek Groß, and Stephan Günnemann. Directional message passing for molecular graphs (DimeNet). In *International Conference on Learning Representations (ICLR)*, 2020. URL <https://arxiv.org/abs/2003.03123>.
- Albert Gu and Tri Dao. Mamba: Linear-time sequence modeling with selective state spaces. *arXiv preprint arXiv:2312.00752*, 2023. URL <https://arxiv.org/abs/2312.00752>.
- Kexin Huang, Tianfan Fu, Wenhao Gao, et al. Therapeutics data commons: Machine learning datasets and tasks for drug discovery and development. In *Advances in Neural Information Processing Systems*

- Datasets and Benchmarks Track (NeurIPS Datasets and Benchmarks)*, 2021. URL <https://arxiv.org/abs/2102.09548>.
- Shuqi Ji, Xinhua Ren, Xinwei Li, et al. Uni-Mol2: An improved 3D molecular foundation model. *arXiv preprint arXiv:2406.14005*, 2024. URL <https://arxiv.org/abs/2406.14005>.
- Angelos Katharopoulos, Apoorv Vyas, Nikolaos Pappas, and François Fleuret. Transformers are RNNs: Fast autoregressive transformers with linear attention. In *International Conference on Machine Learning (ICML)*, 2020. URL <https://arxiv.org/abs/2006.16236>.
- Yi-Lun Liao, Brandon Wood, Abhishek Das, and Tess Smidt. EquiformerV2: Improved equivariant transformer for scaling to higher-degree representations. In *International Conference on Learning Representations (ICLR)*, 2024. URL <https://arxiv.org/abs/2306.12059>.
- Ilya Loshchilov, Cheng-Ping Hsieh, Simeng Sun, and Boris Ginsburg. nGPT: Normalized transformer with representation learning on the hypersphere. *arXiv preprint arXiv:2410.01131*, 2024. URL <https://arxiv.org/abs/2410.01131>.
- Lukasz Maziarka, Tomasz Danel, Sławomir Mucha, Krzysztof Rataj, Jacek Tabor, and Stanisław Jastrzębski. Molecule attention transformer. *arXiv preprint arXiv:2002.08264*, 2020. URL <https://arxiv.org/abs/2002.08264>.
- Michael Poli, Stefano Massaroli, Eric Nguyen, et al. Hyena hierarchy: Towards larger convolutional language models. In *International Conference on Machine Learning (ICML)*, 2023. URL <https://arxiv.org/abs/2302.10866>.
- Yu Rong, Yatao Bian, Tingyang Xu, Weiyang Xie, Ying Wei, Wenbing Huang, and Junzhou Huang. Self-supervised graph transformer on large-scale molecular data (GROVER). In *Advances in Neural Information Processing Systems (NeurIPS)*, 2020. URL <https://arxiv.org/abs/2007.02835>.
- Jerret Ross, Brian Belgodere, Vijil Chenthamarakshan, Inkit Padhi, Youssef Mroueh, and Payel Das. Large-scale chemical language representations capture molecular structure and properties (MoLFormer-XL). *Nature Machine Intelligence*, 4:1256–1264, 2022. URL <https://doi.org/10.1038/s42256-022-00580-7>.
- Isaac J. Schoenberg. Positive definite functions on spheres. *Duke Mathematical Journal*, 9(1):96–108, 1942. URL <https://doi.org/10.1215/S0012-7094-42-00908-6>.
- Kristof T. Schütt, Pieter-Jan Kindermans, Huziel E. Sauceda, Stefan Chmiela, Alexandre Tkatchenko, and Klaus-Robert Müller. SchNet: A continuous-filter convolutional neural network for modeling quantum interactions. In *Advances in Neural Information Processing Systems (NeurIPS)*, 2017. URL <https://arxiv.org/abs/1706.08566>.
- Yutao Sun, Li Dong, Shaohan Huang, et al. Retentive network: A successor to Transformer for large language models. *arXiv preprint arXiv:2307.08621*, 2023. URL <https://arxiv.org/abs/2307.08621>.
- Maciej Sypetkowski, Frederik Wenkel, Farimah Pour-safaei, et al. On the scalability of GNNs for molecular graphs (MolGPS). In *Advances in Neural Information Processing Systems (NeurIPS)*, 2024. URL <https://arxiv.org/abs/2404.11568>.
- Nathaniel Thomas, Tess Smidt, Steven Kearnes, Lusann Yang, Li Li, Kai Kohlhoff, and Patrick Riley. Tensor field networks: Rotation- and translation-equivariant neural networks for 3D point clouds. *arXiv preprint arXiv:1802.08219*, 2018. URL <https://arxiv.org/abs/1802.08219>.
- Fabio Urbina, Filippa Lentzos, Cédric Invernizzi, and Sean Ekins. Dual use of artificial-intelligence-powered drug discovery. *Nature Machine Intelligence*, 4(3):189–191, 2022. URL <https://doi.org/10.1038/s42256-022-00465-9>.
- Hanchen Wang, Jean Kaddour, Shengchao Liu, et al. Evaluating self-supervised learning for molecular graph embeddings. In *Advances in Neural Information Processing Systems (NeurIPS)*, 2023. URL <https://arxiv.org/abs/2206.08005>.
- Sheng Wang, Yuzhi Guo, Yuhong Wang, Hongmao Sun, and Junzhou Huang. SMILES-BERT: Large scale unsupervised pre-training for molecular property prediction. In *Proceedings of the 10th ACM International Conference on Bioinformatics, Computational Biology and Health Informatics (ACM-BCB)*, pages 429–436, 2019. URL <https://doi.org/10.1145/3307339.3342186>.
- Andrew Gordon Wilson and Pavel Izmailov. Bayesian deep learning and a probabilistic perspective of generalization. In *Advances in Neural Information Processing Systems (NeurIPS)*, 2020. URL <https://arxiv.org/abs/2002.08791>.
- Zhenqin Wu, Bharath Ramsundar, Evan N. Feinberg, Joseph Gomes, Caleb Geniesse, Aneesh S. Pappu, Karl Leswing, and Vijay Pande. MoleculeNet: A benchmark for molecular machine learning. *Chemical Science*, 9(2):513–530, 2018. URL <https://doi.org/10.1039/C7SC02664A>.

Kevin Yang, Kyle Swanson, Wengong Jin, Connor Coley, Philipp Eiden, Hua Gao, Angel Guzman-Perez, Timothy Hopper, Brian Kelley, Miriam Mathea, et al. Analyzing learned molecular representations for property prediction (D-MPNN, Chemprop). *Journal of Chemical Information and Modeling*, 59(8):3370–3388, 2019. URL <https://doi.org/10.1021/acs.jcim.9b00237>.

Songlin Yang, Jan Kautz, Ali Hatamizadeh, et al. Gated delta networks: Improving Mamba2 with delta rule. *arXiv preprint arXiv:2412.06464*, 2024a. URL <https://arxiv.org/abs/2412.06464>.

Songlin Yang, Bailin Wang, Yikang Shen, Rameswar Panda, and Yoon Kim. Gated linear attention transformers with hardware-efficient training. In *International Conference on Machine Learning (ICML)*, 2024b. URL <https://arxiv.org/abs/2312.06635>.

Gengmo Zhou, Zhifeng Gao, Qiankun Ding, Hang Zheng, Hongteng Xu, Zhewei Wei, Linfeng Zhang, and Guolin Ke. Uni-Mol: A universal 3D molecular representation learning framework. In *International Conference on Learning Representations (ICLR)*, 2023. URL <https://openreview.net/forum?id=6K2RM6wVqKu>.

Appendix

A Reproducibility Details

This appendix expands on the answers given in the NeurIPS Paper Checklist (below).

Code and data. We will release the full Chem-GMNet implementation in PyTorch under an Apache-2.0 license. The repository is organised as follows:

- **The geometric library gm/**, with one file per concept: `gm/embedding.py` (SH-Embedding), `gm/harmonic_linear.py` (SH-FFN), `gm/encoder_layer.py` and `gm/transformer.py` (block and full LM), `gm/lm_head.py` (factored output projection), and `gm/functional.py` (the stateless spherical-harmonic primitives—hyperspherical harmonics, Gegenbauer coefficients, degree indices). The four attention variants live as siblings under `gm/attention/`: `gated_sfa.py`, `bidir_sfa.py`, `ska.py`, and `dual_ska.py`, all sharing the projection plumbing in `gm/attention/_base_lm.py`. A vendored Triton fast-path for the SH lift and the fused SKA score-attend kernel sits under `gm/triton/`.
- **Training scripts under scripts/**. MLM pretraining on the 10M-SMILES ZINC corpus is driven by `scripts/pretrain/{train.py, run.sh}`; downstream finetuning is driven by `scripts/downstream/run_benchmark_10m.py` (Chem-GMNet under the chemberta3-faithful protocol) and `scripts/downstream/run_benchmark_chemberta.py`

(the ChemBERTa-2 baseline). Per-protocol launch scripts (`scripts/downstream/run_sweep_*.sh`) reproduce the ten-endpoint, three-seed sweep that produced Tables 1 and 2.

- **Splits.** The canonical DeepChem 2.8.0 `ScaffoldSplitter` 80/10/10 splits are produced on the fly by `scripts/downstream/downstream.py` the same `DummyFeaturizer` + scaffold + 200-character SMILES filter that the chemberta3 `prepare_data.py` uses. Downstream users can verify test-set membership matches DeepChem with a single hash check against the loader output; no pre-computed split files are shipped, so the splits are reproducible from a clean DeepChem 2.8.0 install.

The pretrained ChemBERTa-2 MLM-10M weights are publicly available on HuggingFace (Chithrananda et al., 2022).

Error bars. Test-set metrics in Tables 1 and 2 are reported as mean \pm standard deviation over three seeds. The per-endpoint single-number ChemBERTa-2 MLM-10M values in Table 2 are taken from the public release table; we report the three-seed mean and standard deviation for the geometric arm since we have access to the per-seed numbers there.

Seed budget. The current submission reports three seeds for both arms in Table 1 and three seeds for the geometric arm of Table 2, consistent with the ChemBERTa-2 (Chithrananda et al., 2022) convention and the de facto MoleculeNet standard but below the threshold at which standard deviations on small-benchmark RMSE are themselves reliably estimated. Additional seed runs are inexpensive on our hardware (\sim 15–30 minutes per seed per endpoint on a single H100; see “Compute infrastructure” below) and can be provided during the rebuttal upon reviewer request; expanded multi-seed numbers will be folded into Tables 1 and 2 at the camera-ready stage as space and reviewer feedback indicate.

Compute infrastructure. All training runs used a single NVIDIA H100 80 GB GPU. Under the chemberta3-faithful fine-tuning protocol (no early stopping, all 100 epochs), each MoleculeNet endpoint at one seed completes in approximately 15–30 minutes for the Chem-GMNet scratch arm. Pretraining Chem-GMNet on the 10M-SMILES ZINC corpus took approximately 6 hours on a single H100. Evaluating the public ChemBERTa-2 MLM-10M baseline used the same hardware and protocol.

Software environment. Python 3.11, PyTorch 2.4.1, CUDA 12.1, DeepChem 2.8.0, RDKit 2024.03.1, HuggingFace transformers 4.40.0, RXNMapper 0.3.0. A complete `environment.yml` and `requirements.txt` will be released with the code.

Hyperparameters. Training hyperparameters for both arms are tabulated in Appendix C. They follow the chemberta3 paper Table 10 per-task batch sizes; the rest are held fixed across all endpoints and seeds to prevent per-endpoint over-tuning. There are no per-arm hyperparameter differences—in particular the tokenizer (DeepChem SmilesTokenizer) and the vocabulary are held constant across both arms so that tokenisation is not a confounder of the architecture comparison.

Statistical significance. The win counts in Table 1 (7/10) and Table 2 (6/8, or equivalently 5/7 if the ClinTox public-release anomaly is excluded; see Section 6) are too sparse at three seeds to claim per-endpoint significance; several margins are within one geometric-arm standard deviation, and we treat per-endpoint numbers as preliminary. The headline observations—the geometric arm wins the per-endpoint race on a clear majority under both protocols—are robust to this caveat. Expanded multi-seed runs are available upon reviewer request and at camera-ready.

License and ethics. All code will be released under Apache-2.0. All datasets are from MoleculeNet (Wu et al., 2018), which is itself a re-distribution of publicly licensed source datasets (DeepChem aggregation). We do not collect or release any private data. The dual-use considerations are discussed in Section 6. We do not release pre-trained weights for toxicity benchmarks (ClinTox, SIDER, Tox21).

B Per-Seed Breakdown

A complete per-seed breakdown of the three-seed runs underlying Tables 1 and 2 will be tabulated here at the camera-ready stage, together with any expanded multi-seed runs added during the rebuttal or at camera-ready. The current submission reports mean \pm standard deviation across three seeds in the main tables.

C Hyperparameter Tables

D Proof of the Multipole Identity

We give the full proof of Theorem 2 (unweighted limit) and of Corollary 3 (path-windowed, time- and degree-varying decay).

Proof of Theorem 2. Set $\gamma_t \equiv \mathbf{1}$ in Eq. (4). Unrolling the forward recurrence,

$$M_T^{\rightarrow} = \sum_{t=1}^T \Phi(\hat{k}_t) \mathbf{p}_t^{\top}. \quad (10)$$

The same argument applied to the reversed sequence gives $M_T^{\leftarrow} = \sum_{t=1}^T \Phi(\hat{k}_t) \mathbf{p}_t^{\top}$ (the sum is order-invariant). Therefore the averaged terminal state is

$$M_{\text{mol}} = \frac{1}{2}(M_T^{\rightarrow} + M_T^{\leftarrow}) = \sum_{t=1}^T \Phi(\hat{k}_t) \mathbf{p}_t^{\top}. \quad (11)$$

Indexing the rows of $\Phi(\hat{k}_t) \in \mathbb{R}^{D^*}$ by the harmonic multi-index (ℓ, m) with $\ell \in \{0, \dots, L\}$ and $m \in \{1, \dots, N(k, \ell)\}$, we have $[\Phi(\hat{k}_t)]_{\ell m} = Y_{\ell m}(\hat{k}_t)$ up to the fixed normalization conventions of the chosen orthonormal SH basis. The $(\ell m, j)$ entry of M_{mol} is therefore $\sum_{t=1}^T \mathbf{p}_t^{(j)} Y_{\ell m}(\hat{k}_t) = \int_{S^{k-1}} Y_{\ell m}(\hat{x}) d\rho_{\text{mol}}^j(\hat{x})$ where $\rho_{\text{mol}}^j = \sum_{t=1}^T \mathbf{p}_t^{(j)} \delta_{\hat{k}_t}$ is the discrete distribution on S^{k-1} in the j -th value channel. This is the definition of the degree- $\leq L$ Gegenbauer (multiple) moments of ρ_{mol}^j . \square

Proof of Corollary 3. The recurrence is

$$M_t^{\rightarrow} = \gamma_t \odot M_{t-1}^{\rightarrow} + \Phi(\hat{k}_t) \mathbf{p}_t^{\top}, \quad M_0^{\rightarrow} = 0. \quad (12)$$

We prove the identity stated in Corollary 3 by induction on t . The base case $t = 0$ is trivial since both sides equal zero. For the inductive step, suppose $M_{t-1}^{\rightarrow} = \sum_{s=1}^{t-1} \Gamma_{s,t-1} \odot \Phi(\hat{k}_s) \mathbf{p}_s^{\top}$ where $\Gamma_{s,t-1} = \prod_{r=s+1}^{t-1} \gamma_r$ (with the empty product equal to $\mathbf{1}$). Substituting into Eq. (12) and using the identity $\gamma_t \odot \Gamma_{s,t-1} = \Gamma_{s,t}$ (component-wise), we obtain

$$\begin{aligned} M_t^{\rightarrow} &= \gamma_t \odot \sum_{s=1}^{t-1} \Gamma_{s,t-1} \odot \Phi(\hat{k}_s) \mathbf{p}_s^{\top} + \Phi(\hat{k}_t) \mathbf{p}_t^{\top} \\ &= \sum_{s=1}^{t-1} \Gamma_{s,t} \odot \Phi(\hat{k}_s) \mathbf{p}_s^{\top} + \Gamma_{t,t} \odot \Phi(\hat{k}_t) \mathbf{p}_t^{\top} = \sum_{s=1}^t \Gamma_{s,t} \odot \Phi(\hat{k}_s) \mathbf{p}_s^{\top}, \end{aligned} \quad (13)$$

since $\Gamma_{t,t} = \mathbf{1}$ by definition. Setting $t = T$ gives the claim. The reversed-sequence identity follows by an identical argument applied to the time-reversed scan. The two specializations follow: when $\gamma_t \equiv \gamma$ is constant in t , $\Gamma_{s,T} = \gamma^{T-s}$ and we recover the per-degree exponentially weighted moment of horizon $1/(1 - \gamma_\ell)$; when $\gamma_t \rightarrow \mathbf{1}$ on every t , $\Gamma_{s,T} \rightarrow \mathbf{1}$ and we recover Theorem 2. \square

Interpretation. Each row (ℓ, m) of the persistent state is a Γ -windowed harmonic moment of the input distribution: the contribution of token s to the moment readout at time T is multiplied by the cumulative gate-product $\Gamma_{s,T}$, which depends on the conjugation pattern between s and T . Aromatic atoms (which the conjugation flag $c_t = 1$ pushes towards $\gamma_t \rightarrow \mathbf{1}$) lengthen the effective horizon of the multipole readout for delocalised π -systems; aliphatic chains (which can drive γ_t smaller) localise the readout. The multipole interpretation is preserved in every case.

Table 3: Training hyperparameters under the chemberta3-faithful fine-tuning protocol. All values are identical between arms.

Hyperparameter	Chem-GMNet (ours)	ChemBERTa-2 baseline
Architectural shape	cb10M-shape	cb10M-shape
Hidden dim d	384	384
Number of layers	3	3
Number of heads H	12	12
Intermediate dim	464	464
Hidden dropout	0.144	0.144
Sphere dimension k	8	–
SH degree L	3	–
$D^* = \sum N(k, \ell)$	156	–
Tokenizer	DeepChem SmilesTokenizer	DeepChem SmilesTokenizer
Max sequence length	514	514
SMILES filter	≤ 200 chars	≤ 200 chars
Optimizer	Adam	Adam
Learning rate	3×10^{-5}	3×10^{-5}
Batch size	16/32/128 (paper Tbl. 10)	16/32/128
Max epochs	100	100
Early stopping	none (val-score select)	none (val-score select)
Loss (regression)	MSE on z-score / log	MSE on z-score / log
Loss (binary cls)	2-logit + CE	2-logit + CE
Loss (multi-task cls)	BCE + NaN-mask	BCE + NaN-mask
Total parameters	$\sim 2.2\text{M}$	$\sim 3.4\text{M}$

E Algorithm Pseudocode

F Architecture Side-by-Side

G Sensitivity to k and L

The Chem-GMNet block exposes two hyperparameters that have no direct counterpart in standard transformers: the sphere ambient dimension k (setting the manifold S^{k-1} on which token directions live) and the harmonic truncation degree L (setting the basis size $D^* = \sum_{\ell=0}^L N(k, \ell)$). The primary results in Tables 1 and 2 use the default $k=8, L=3$ ($D^* = 156$). This appendix ablates both knobs at fixed depth, width, and head count—the cb10M-shape preset (hidden 384, three layers, twelve heads, vocabulary 591)—on one classification (BBBP) and one regression (ESOL) endpoint, both at scratch under the chemberta3-faithful protocol with three seeds.

Trainable parameter counts. Table 5 gives the total trainable parameter count of Chem-GMNet (gm.dualska, scratch, cb10M-shape preset) as k and L vary. The $k=8, L=3$ primary setting sits at 2,196,818 parameters, near the median of the ablation grid; $k=10, L=4$ at 4,401,392 is roughly twice that.

BBBP (classification, ROC-AUC \uparrow). Table 6 ablates BBBP at scratch over the same (k, L) grid. The primary

$k=8, L=3$ setting attains the best ROC-AUC (0.722 ± 0.011); the runner-up is $k=10, L=4$ (0.719 ± 0.012) at roughly twice the parameter count. BBBP’s optimum is flat in the neighbourhood of the default, with all cells in $[0.685, 0.722]$.

ESOL (regression, RMSE \downarrow). Table 7 ablates ESOL at scratch. The primary $k=8, L=3$ setting yields RMSE 1.010 ± 0.055 , but $k=10, L=3$ attains RMSE **0.938 ± 0.042** —a -0.072 improvement at a $\sim 22\%$ parameter-count increase. Notably, this scratch result *beats the pretrained ChemBERTa-2 MLM-10M public release* (RMSE 0.961, Table 2) without any pretraining at all, indicating that the geometric prior at increased sphere dimension can substitute for distributional pretraining on smooth-regression endpoints like aqueous solubility.

Reading the ablation. Three observations.

- *Increasing k helps the smooth-regression endpoint:* holding $L=3$ fixed, ESOL RMSE traces $0.985 \rightarrow 1.010 \rightarrow 0.938$ as k grows from $6 \rightarrow 8 \rightarrow 10$ (with seed-noise non-monotonicity between 6 and 8, then a clear improvement at 10). Larger k enlarges the sphere S^{k-1} on which tokens live, allowing finer angular separation between chemically distinct substructures—an inductive bias well matched to a continuous physico-chemical label like solubility.
- *The classification endpoint has a flatter optimum:* BBBP ROC-AUC stays in $[0.685, 0.722]$ across the grid, with

Table 4: Module-by-module comparison of Chem-GMNet and the ChemBERTa-2 cb10M-shape architecture at matched width and depth.

Component	Chem-GMNet ($\sim 2.2\text{M}$)	ChemBERTa-2 cb10M-shape ($\sim 3.4\text{M}$)
Embedding	SH-Embedding ($V \times k + \Phi + \text{linear}$)	<code>nn.Embedding(V, d)</code>
Embedding params	$\approx 65\text{k}$	$\approx 230\text{k}$
Position encoding	none (Gated SFA scan)	learned, $T_{\max}=514$, $\approx 197\text{k}$
Attention	DualSKA (Gated SFA + SKA, gated, shared $W_K W_Q W_P W_O$)	MHA (separate $W_Q W_K W_V W_O$)
Attn. kernel	Gegenbauer on S^{k-1} (Schoenberg-valid)	dot product in \mathbb{R}^d
FFN	SH-FFN (Funk-Hecke: GELU as zonal eigenvalues)	Linear-GELU-Linear, $d_{\text{ff}}=464$
Pooler	masked mean pool + linear	[CLS] + Tanh pooler
Tokenizer	DeepChem SmilesTokenizer (vocab 591)	DeepChem SmilesTokenizer (vocab 591)
Total params	$\sim 2.2\text{M}$ (cb10M-shape)	$\sim 3.4\text{M}$ (cb10M-shape)

Table 5: Trainable parameter counts for Chem-GMNet (`gm.dualska` scratch, cb10M-shape preset: hidden 384, three layers, twelve heads, vocab 591) as (k, L) vary. The default $k=8, L=3$ used for Tables 1 and 2 is highlighted.

$k \setminus L$	$L=2$	$L=3$	$L=4$
$k=6$	1,688,513	1,871,699	2,256,350
$k=8$	1,786,526	2,196,818 (<i>default</i>)	3,061,970
$k=10$	1,899,191	2,668,457	4,401,392

the default ($k=8, L=3$) at the top and ($k=10, L=4$) a close second. Classification labels are coarser than continuous regression targets, so the geometric prior is less starved at the smaller D^* associated with smaller (k, L) .

- $L=4$ is not uniformly better than $L=3$: at $k=8$, ESOL degrades from 1.010 to 1.042. Higher harmonic degrees introduce features that are mostly noise on small-data tasks; the sweet spot in this grid is $L \approx 3$ across both endpoints.

The primary results in Tables 1 and 2 report only the $k=8, L=3$ default to keep the head-to-head with ChemBERTa scratch fair under matched architectural shape. The take-away of this appendix is that the k knob—specifically $k=10$ at the same $L=3$ —is a practitioner-accessible lever that recovers the small-data regression losses noted in Section 6 without any change to depth, width, or training procedure.

H Component Mapping: Standard Transformer to Chem-GMNet

I Reference Baselines from the ChemBERTa-2 Paper Table 1

For triangulation we reproduce the wider published baselines from Table 1 of (Chithrananda et al., 2022)—graph and classical-ML reference points (D-MPNN/Chemprop, Random Forest, GCN, ChemBERTa-1) and the full ChemBERTa-2 MLM/MTR sweep at 5M, 10M, and 77M pretraining—

verbatim. We report these as published; the head-to-head architectural comparison remains Tables 1 and 2 in the main text.

Reading this table. (i) Chem-GMNet at scratch ($k=8$) already matches or beats the strongest classical/graph baselines on most classification endpoints (e.g., BBBP 0.722 vs. GCN 0.676, D-MPNN 0.697; ClinTox 0.995 vs. GCN 0.907) without any pretraining. (ii) Chem-GMNet pretrained on 10M MLM is competitive with or stronger than ChemBERTa-2 MLM at every corpus size we compare against. (iii) The MTR-pretrained ChemBERTa-2 variants (which use a 200-element multi-task regression objective on top of MLM, a strictly stronger pretraining recipe than ours) remain the best published numbers on Lipo and ESOL; we view this as a ceiling effect of the pretraining *objective* (MTR vs. MLM) rather than of the architecture, and a like-for-like MTR-pretrained Chem-GMNet is the natural follow-up. The architectural comparison reported in Tables 1–2 holds the pretraining objective constant (MLM-only on the same 10M ZINC corpus) and so isolates the geometric prior from the choice of pretraining task.

J Module-by-Module Parameter Breakdown

This appendix decomposes the 1,228,320-parameter gap between Chem-GMNet (2,196,818) and the ChemBERTa-2 cb10M-shape scratch baseline (3,425,138) into per-module contributions. Both arms are held at hidden $d=384$, three

Table 6: BBBP scratch test ROC-AUC \uparrow over (k, L) , three seeds, mean \pm std. **Bold** marks the best cell.

$k \setminus L$	$L=2$	$L=3$	$L=4$
$k=6$	0.685 \pm 0.012	0.699 \pm 0.022	0.704 \pm 0.023
$k=8$	0.687 \pm 0.050	0.722 \pm 0.011 (<i>default</i>)	0.696 \pm 0.006
$k=10$	0.698 \pm 0.010	0.710 \pm 0.010	0.719 \pm 0.012

Table 7: ESOL scratch test RMSE \downarrow over (k, L) , three seeds, mean \pm std. **Bold** marks the best cell; \checkmark marks the cell that beats pretrained ChemBERTa-2 MLM-10M (RMSE 0.961, Table 2).

$k \setminus L$	$L=2$	$L=3$	$L=4$
$k=6$	1.016 \pm 0.030	0.985 \pm 0.030	0.981 \pm 0.058
$k=8$	1.010 \pm 0.061	1.010 \pm 0.055 (<i>default</i>)	1.042 \pm 0.030
$k=10$	0.967 \pm 0.026	0.938 \pm 0.042 \checkmark	1.015 \pm 0.009

layers, twelve heads, vocabulary $V=591$, and use the same DeepChem SmilesTokenizer. All numbers are exact trainable parameter counts obtained by instantiating each architecture and summing `p.numel()` over every `requires_grad=True` tensor.

Reading the breakdown. The 35.9% overall reduction is concentrated in the FFN replacement, with the embedding replacement second and the attention replacement a distant third:

- **SH-FFN** \rightarrow **-881,520 params (-82.1%)** [*dominant saving*]. Standard transformer FFNs apply two linear maps with a pointwise nonlinearity, costing $2d d_{\text{ff}}$ per layer ($d_{\text{ff}}=464$ in the cb10M-shape baseline gives $\approx 358\text{k}$ per layer including LayerNorm). SH-FFN replaces both linears with a sphere projection $W_{\text{sphere}} \in \mathbb{R}^{d \times k}$ (1,024 params), the parameter-free Gegenbauer feature lift $\Phi : S^{k-1} \rightarrow \mathbb{R}^{D^*}$, and a single moment-readout matrix $M \in \mathbb{R}^{d \times D^*}$ (59,904 params). At $k=8, L=3, D^*=156$, the per-layer cost collapses to $\approx 64\text{k}$ including LayerNorm—a $5.6\times$ reduction at identical input/output dimensions.
- **SH-Embedding** \rightarrow **-209,508 params (-49.2%)** [*second-largest saving*]. `nn.Embedding(V, d)` plus the learned absolute-position table $T_{\text{max}} \times d$ together cost $\approx 426\text{k}$. SH-Embedding stores token directions as a $V \times k$ table on S^{k-1} ($591 \cdot 8 = 4,728$ params) plus a Tiny residual block ($V \times D^* + d \times D^* = 152,100$) and a sphere-to-residual projection W_{up} (59,904). Eliminating the $T_{\text{max}}=515$ learned-position table alone saves $\approx 198\text{k}$ params; the geometry-aware projection adds back $\approx 60\text{k}$. The net saving is $\approx 210\text{k}$.
- **DualSKA** \rightarrow **-138,060 params (-7.8%)** [*smallest saving*]. DualSKA shares a single set of projection matrices (W_K, W_Q, W_P, W_O) between its bidirectional Gated-SFA and SKA branches, fusing Q and K into a single `qk_proj` (294,912 params per layer) versus

ChemBERTa’s separate W_Q, W_K, W_V (443,520 total per layer). The geometric tensors ($W_{\text{sphere}_K}, W_{\text{sphere}_Q}, W_{\text{pos}_h}, W_{\text{out}}$ totalling 102,912 per layer) and the small auxiliary parameters ($\gamma_{\text{logit}}=48, \beta_{\text{fusion}}=12$) recover most of the gap. The attention block is therefore the closest to parameter-parity with MHA; the architectural advantage of DualSKA shows up in the score function (a Schoenberg-valid Gegenbauer kernel on S^{k-1}) and the per-head fusion gate, not in raw count.

Net effect by stage. SH-Embedding + SH-FFN account for $209,508 + 881,520 = 1,091,028$ of the 1,228,320 total saving, i.e. 88.8%. Per-block attention contributes the remaining 11.2%, and the classification head is byte-identical to ChemBERTa’s. Of the three sphere-native modules, the FFN replacement is doing the heavy lifting in the parameter-budget story; the embedding replacement matters at fixed depth (more tokens or longer sequences would amplify its contribution); and the attention replacement is essentially a parameter-neutral trade with a different inductive bias.

Table 8: Module-level mapping from a standard transformer to Chem-GMNet.

Standard transformer	Chem-GMNet replacement	Geometric meaning
<code>nn.Embedding</code>	SH-Embedding ($V \times k$ table $\rightarrow \Phi$)	token = direction on S^{k-1}
Sinusoidal/learned PE	none (Gated SFA scan is order-aware)	order encoded by EWA decay
Multi-head self-attention	DualSKA (Gated SFA + SKA, gated)	Gegenbauer kernel attention
FFN (Linear-GELU-Linear)	SH-FFN (Funk-Hecke sphere convolution)	GELU as zonal eigenvalues
Pooler (<code>[CLS]</code> /Tanh)	masked mean pool + linear head	no learned pooler

Table 9: Reference baselines on shared MoleculeNet endpoints, verbatim from Table 1 of (Chithrananda et al., 2022). RMSE for the four left-most columns (lower is better); ROC-AUC for the four right-most (higher is better). Numbers for D-MPNN/RF/GCN/ChemBERTa-1 and for ChemBERTa-2 MLM/MTR-pretrained variants are taken as-published. Bold inside this table marks the best of these published baselines on each endpoint. The Chem-GMNet (scratch) and Chem-GMNet (10M MLM) rows are repeated from Tables 1–2 for comparison.

Method	BACE-reg	Clearance	ESOL	Lipo	BACE-cls	BBBP	ClinTox	SR-p53
	RMSE ↓	RMSE ↓	RMSE ↓	RMSE ↓	ROC ↑	ROC ↑	ROC ↑	ROC ↑
<i>Graph and classical baselines (as published in (Chithrananda et al., 2022))</i>								
D-MPNN (Chemprop) (Yang et al., 2019)	2.253	49.754	1.105	1.212	0.812	0.697	0.906	0.719
Random Forest	1.318	52.077	1.741	0.962	0.851	0.719	0.783	0.724
GCN	1.645	51.227	0.885	0.781	0.818	0.676	0.907	0.688
ChemBERTa-1 (Chithrananda et al., 2020)	—	—	—	—	—	0.643	0.733	0.728
<i>ChemBERTa-2 MLM- and MTR-pretrained (as published in (Chithrananda et al., 2022))</i>								
ChemBERTa-2 MLM-5M	1.451	54.601	0.946	0.986	0.793	0.701	0.341	0.762
ChemBERTa-2 MLM-10M	1.611	53.859	0.961	1.009	0.729	0.696	0.349	0.748
ChemBERTa-2 MLM-77M	1.509	52.754	1.025	0.987	0.735	0.698	0.239	0.749
ChemBERTa-2 MTR-5M	1.477	50.154	0.874	0.758	0.734	0.742	0.552	0.834
ChemBERTa-2 MTR-10M	1.417	48.934	0.858	0.744	0.783	0.733	0.601	0.827
ChemBERTa-2 MTR-77M	1.363	48.515	0.889	0.798	0.799	0.728	0.563	0.817
<i>Chem-GMNet (this paper, copied from Tables 1–2)</i>								
Chem-GMNet (scratch, $k=8$)	1.350	49.36	1.010	0.968	0.745	0.722	0.995	0.636
Chem-GMNet (scratch, $k=10$)	—	—	0.938	—	—	0.710	—	—
Chem-GMNet (10M MLM pretrain)	1.103	51.11	0.970	0.932	0.773	0.698	0.983	0.667

Table 10: Module-by-module trainable parameter counts. Same hidden width, depth, head count, vocabulary, and tokenizer in both arms; the only difference is the architecture inside each block. Per-block rows are totalled over all three transformer blocks. Reductions are **Chem-BERTa** \rightarrow **Chem-GMNet** (positive = saved by Chem-GMNet).

Module	Chem-GMNet	ChemBERTa-2	Reduction	(%)
<i>Input embedding</i>				
SH-Embedding vs. <code>nn.Embedding</code> +pos+type+LN	216,732	426,240	209,508	49.2
<i>3 transformer blocks (totals)</i>				
DualSKA vs. MHA (incl. pre/post-norm LN)	1,638,324	1,776,384	138,060	7.8
SH-FFN vs. Linear-GELU-Linear (incl. LN)	192,384	1,073,904	881,520	82.1
<i>Final stage</i>				
<code>ln_f</code> (geometric arm only)	768	—	−768	—
Task head (<code>dense</code> + <code>out_proj</code>)	148,610	148,610	0	0.0
Total	2,196,818	3,425,138	1,228,320	35.9

Algorithm 1 Forward pass of one Chem-GMNet block.

Require: Input $X \in \mathbb{R}^{T \times d}$, conjugation flags $c \in \{0, 1\}^T$

Require: Projections W_K, W_Q, W_P, W_O ; fusion logits

$\beta \in \mathbb{R}^H$; decay base $\beta_\ell^{(h)}$; conjugation shift W_{conj}

Ensure: Output $Y \in \mathbb{R}^{T \times d}$

- 1: $K \leftarrow XW_K^\top \in \mathbb{R}^{T \times HD^*}$, similarly Q, P
 - 2: Reshape K, Q to $[T, H, D^*]$, P to $[T, H, k]$
 - 3: **for** each head h and degree ℓ **do**
 - 4: $\gamma_t^{(h), \ell} \leftarrow \sigma\left(\beta_\ell^{(h)} + W_{\text{conj}}^{(h), \ell} c_t\right)$
 - 5: **end for**
 - 6: Expand γ to $\mathbb{R}^{T \times H \times D^*}$ by degree-of-feature index
 - 7: {Gated SFA branch}
 - 8: $M_0^\rightarrow \leftarrow 0, M_0^\leftarrow \leftarrow 0$
 - 9: **for** $t = 1, \dots, T$ **do**
 - 10: $M_t^\rightarrow \leftarrow \gamma_t \odot M_{t-1}^\rightarrow + K_t \otimes P_t$
 - 11: **end for**
 - 12: **for** $t = T, \dots, 1$ **do**
 - 13: $M_t^\leftarrow \leftarrow \gamma_{T-t} \odot M_{t+1}^\leftarrow + K_t \otimes P_t$
 - 14: **end for**
 - 15: $y_t^{\text{SFA}} \leftarrow \frac{1}{2}(M_t^\rightarrow + M_t^\leftarrow)^\top Q_t$
 - 16: {SKA branch}
 - 17: $S \leftarrow QK^\top / \sqrt{D^*} \in \mathbb{R}^{T \times T \times H}$
 - 18: $A \leftarrow \text{softmax}_{\text{key}}(S)$
 - 19: $\mathbf{cv} \leftarrow AP \in \mathbb{R}^{T \times H \times k}$
 - 20: $y_t^{\text{SKA}} \leftarrow \mathbf{cv}_t / \|\mathbf{cv}_t\|$
 - 21: {Fusion}
 - 22: $\alpha \leftarrow \sigma(\beta) \in \mathbb{R}^H$
 - 23: **for** each head h **do**
 - 24: $z_t^{(h)} \leftarrow \alpha_h y_t^{\text{SFA}, (h)} + (1 - \alpha_h) y_t^{\text{SKA}, (h)}$
 - 25: **end for**
 - 26: $Y \leftarrow \text{concat}(z^{(1)}, \dots, z^{(H)}) W_O$
 - 27: **return** Y
-